Daytime SNR modeling of GEOs in the SWIR for low-cost, ground-based imaging

Grant M. Thomas

Air Force Institute of Technology, Wright-Patterson AFB, Ohio

Richard G. Cobb

Air Force Institute of Technology, Wright-Patterson AFB, Ohio

ABSTRACT

Ground-based short-wave infrared (SWIR) imaging is a low-cost and informative method of daytime Geosynchronous (GEO) satellite detection and characterization. However, for large solar phase angles, spectral sky brightness and low satellite reflected signal combine to make this approach more challenging. A generalized model for satellite spectra using diffuse reflection was developed and compared to modeled atmospherics to determine the most promising bands-of-interest. This research will show that SWIR-band imaging offers distinct advantages over the visible for daytime GEO satellite custody and investigate the utility of SWIR band imaging particularly near twilight.

1 INTRODUCTION

Space Situational Awareness (SSA) is defined as the requisite current and predictive knowledge of the space environment and the operational environment upon which space operations depend as well as all factors, activities, and events of friendly and adversary space forces across the spectrum of conflict [4]. SSA is fundamental to conducting space operations as it is *the* enabler for accomplishing all other space control tasks [4]. One specific capability desired by the Air Force Space Command (AFSPC) is that of cost affordable ground-based daylight satellite custody sensors. "Daylight" (used interchangeably with "daytime") is defined as the hours between the end of morning civil twilight and the beginning of evening civil twilight. While it is currently possible to image Earth orbiting objects in the daytime sky with a highly-specialized sensor, cost-effective solutions are sought for widespread implementation and utility. One such solution is to augment ground-based optical telescopes with SWIR sensors to image during twilight and even into daylight hours as opposed merely imaging when the ground site is in darkness.

Custody methods can be divided into two groups by sensor type and collection method: active and passive. Both active and passive methods are necessary to build a robust SSA capability with associated advantages and limitations. Active methods require significant power to operate particularly at higher orbital altitudes as the signal strength diminishes by the quartic of the distance from the sensor to the object. Higher-power required often leads to greater sensor complexity and cost and therefore active collection methods will not be considered for this research. Conversely, passive methods are low-power (comparatively) and have the additional advantage of clandestine collection which is valuable for military purposes. Passive electro-optical (EO) sensors can be divided into categories relating to the detection wavelengths of the sensors: Visible to Near-Infrared (Vis-NIR) from 0.4-1.4μm, Short-Wave Infrared (SWIR) from 1.4-3μm, Medium-Wave Infrared (MWIR) from 3-8μm and Long-Wave Infrared (LWIR) from 8-15μm. The satellite signal is comprised of both an emitted and reflective component. The reflective component of the satellite signal reaches peak power density in the Visible-band due to Wein's Law [7]. Vis-NIR and SWIR sensors are designed to detect this radiation from the Sun reflecting off the satellite surfaces. The emitted signal from the satellite peaks in the LWIR for typical satellite operating temperatures. Vis-SWIR sensors neglect the emitted satellite signal and LWIR sensors neglect the reflected solar radiation. MWIR sensors, though sensitive to both reflected

and emitted satellite signals, are not often used for ground-based resident space object (RSO) detection due to the comparably weak signal strength. Since LWIR sensors rely on the emission rather than reflection from the RSO, detection is possible anytime the satellite is overhead (day or night). However, LWIR sensors must be actively cooled to decrease thermal noise contributions. The associated size and complexity of LWIR sensor systems increase the cost and makes widespread sensor proliferation difficult. Vis-NIR sensors systems are passive, low-cost and relatively high-resolution systems that are currently contributing to a large portion of the useful SSA [11], [9]. However these sensors are only effective during the hours of local darkness for a ground site as the ever brightening sky and atmospheric scattering effects erode higher signal to noise ratios (SNR) for a satellite with the rising Sun. This research will demonstrate that by moving from Vis-NIR to SWIR the sky brightness and atmospheric scattering effects are sufficiently diminished providing a "sweet-spot" for daytime RSO detection.

1.1 Objective

The goal of this research is to extend the custody of GEO objects into daylight hours. While 24/7 imaging is desirable, any extension of the current daytime custody window is of interest particularly for GEO satellites. SSA in all orbit regimes is a concern, but the Air Force Research Laboratory (AFRL) continues to focus on the GEO regime as prime real estate where 800+ satellites reside [15]. Because of the increased distance from the Earth, GEOsats are often dim and/or infrequently observed objects which makes orbital determination difficult and sustainable SSA elusive [2]. In spite of the difficulties, GEO targets are natural candidates for a baseline daylight custody analysis due to their value to the Department of Defense (DoD) and relative fixed position above the local horizon. Unfortunately, daytime SWIR band imaging of GEOsats is not the panacea for persistent SSA. However, as will be shown, SWIR imaging is a critical component of the multi-sensor, hyperspectral network of sensors envisioned for future SSA. By extending the detection window in several SWIR bands, even by minutes as compared to the NIR, this research will demonstrate the efficacy of a cost-effective partial SSA solution.

2 APPROACH

In general, a persistent satellite signal needs to exist above the sky-background noise to be detectable. Since the satellite signal in the Vis-SWIR wavelengths is composed of reflected solar radiation, it is not immediately apparent why looking beyond the visible band is beneficial. However, as the reflected signal diminishes with lessening solar flux into the SWIR, the scattering effects begin to have less of an effect as well. By constructing a simple satellite signal model and comparing to a spectral sky background radiance generated by a first-principle atmospheric modeler such as the Laser Environmental Effects Definition and Reference (LEEDR), one can begin to understand the slightly dimmer (i.e. less-scattered) background makes detection of even a diminished satellite signal possible.

2.1 Satellite Photometry and Signal Model Generation

In the Vis-SWIR bands, satellite photometry is the measurement of reflected Sunlight arriving at a sensor from a distant satellite. The resultant signal is primarily a function of solar phase angle, satellite geometry and pose, material reflectances, and the wavelength of incident radiation.

The irradiance E received at the ground-based telescope is a summation of both the direct solar radiation and indirect radiation from Earth's albedo reflected from the satellite. Both the direct and indirect inputs are functions of the Sun's output energy which can be approximated using the Black-body Planckian function. The radiant exitance M is the flux per unit area leaving a surface of a radiation source. The irradiance E is the flux per unit area received by a surface element [3]. M and E are both given in terms of $(\mathrm{W\,m^{-2}\,\mu m^{-1}})$. By assuming a temperature, the radiant exitance per wavelength, (M), is calculated in Equation 1.

$$M_{sun}(\lambda, T) = \frac{2hc^2}{\lambda^5} \frac{1}{\exp \frac{hc}{\lambda k_B T_{sun}} - 1} \tag{1}$$

Notably for a Lambertian source,

$$M = \pi L \qquad [\mathrm{W\,m^{-2}\,\mu m^{-1}}] \quad (2)$$

and thus

$$L = \frac{M}{\pi} \qquad [\mathrm{W\,m^{-2}\,\mu m^{-1}\,sr^{-1}}] \quad (3)$$

In general, the approach will be to: 1) Calculate the irradiance arriving at the satellite from either the direct or indirect source 2) Determine the orbit, pose, and surface area of the satellite 3) Assume the satellite is a point source relative to the ground site with a derived intensity (from 1 & 2) and 4) calculate the received irradiance at the ground site using diffuse surface reflection.

2.1.1 Direct Solar Illumination

To calculate the direct solar irradiance, the sun is assumed to be a Lambertian source which means that each element of projected area of the sun contributes the same amount of radiant exitance regardless of angle.

$$E_{sun,\lambda_{direct}} = \frac{A_{sun_{proj}} M_\lambda}{\pi R^2_{sun2GEOsat}} = \frac{M_\lambda R^2_{sun}}{R^2_{sun2GEOsat}} \qquad [\mathrm{W\,m^{-2}\,\mu m^{-1}}] \quad (4)$$

The spectral irradiance was calculated for true longitudes, l, (alternate orbital element values for a circular, Equatorial orbit which define orbital positions/slots for GEO satellites) correlating to front, back and side illuminated cases. The dependence of irradiance on a GEO satellite's position within the orbit (in terms of l) is negligible as the distance from the Sun to Earth is much greater than that of the Earth to GEO orbit.

2.1.2 Indirect Solar Illumination

Indirect solar radiation is defined as radiation that is reflected off the Earth's surface (called albedo) and then back "up" towards the satellite. The albedo radiation incident on the satellite depends on the surface-type (ie water, urban or vegetation) of the Earth beneath the satellite at any given time. The albedo radiation is also significantly less than the direct reflected radiation and frequently neglected. However, for daytime GEO satellite imaging, albedo reflectance must be considered as the satellite is often illuminated from behind (backlit) and albedo is a detectable signal mechanism. Equivalently, a large solar phase angle (>90°) is often used to describe the backlit satellite illumination condition. Since the solar panels are facing the Sun to generate power for the spacecraft, the satellite nadir facing bus features and solar panel back faces are illuminated exclusively by the albedo radiation from the Earth. Since the Earth is relatively distant from the satellite at a GEO orbiting altitude, a constant albedo value of 0.3 is often assumed[7] and will be utilized in this model as well. Using Equation 5 the spectral irradiance arriving at the Geostationary satellite due to Earth's albedo ($E_{albedo,\ \lambda}$) is calculated thus:

$$E_{albedo,\lambda} = 0.3 * \frac{M_{sun,\lambda} * R^2_{sun}}{R^2_{sun2Earth}} \qquad [\mathrm{W\,m^{-2}\,\mu m^{-1}}] \quad (5)$$

2.1.3 Solar Phase Angle and Illumination Angle

The SPA and illumination angle (IA) will be defined below to help determine the received radiance from the satellite and the radiance of the sky background. Since the satellite is in constant motion orbiting the Earth and the Earth is in an orbit around the Sun, both SPA and IA will be a function of time of day, day of the year, and ground site latitude. This research will focus on a ground site latitude of 39.76°N latitude and 84.2°W longitude which corresponds to Dayton, OH.

The SPA is the angle between the vector pointing from the satellite to the Sun (aka "Sun vector") and the vector pointing from the satellite to the ground site as shown in Fig. 1. SPA is used to determine the illumination angle for the satellite on orbit from the perspective of the ground site. Additionally, since the normal vector of the solar panels on a GEO satellite are assumed to be co-aligned with the Sun vector (with respect to the satellite), SPA will also define solar panel pose illumination. The satellite bus for this model is assumed to be nadir facing towards Earth's equator.

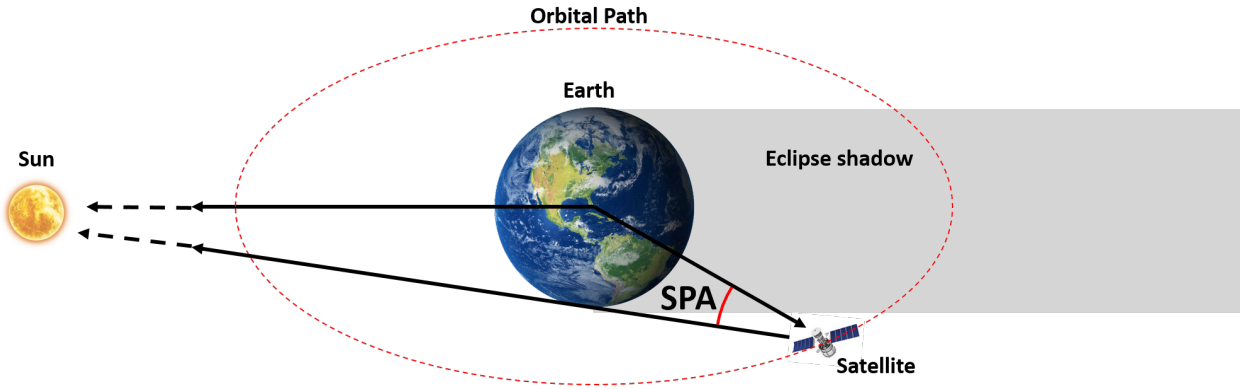

Figure 1: Daytime solar phase angle (SPA) visualization

To determine the SPA quantitatively, it is first necessary to compute the Sun's geocentric position for a given period of time. The Sun position vector is calculated for each Julian Date with respect to the mean equator and equinox of J2000 in the International Celestial Reference Frame which is accurate to within 0.01 sec [16]. Since the ω_{Earth} is equal to ω_{GEO} by definition, the vector positions of a GEO satellite with respect to the center of the Earth "fix" a satellite's position overhead in the GEO-belt. The longitude and latitude of a ground site are determine the ground site location with respect to Earth's center and vector addition is used to determine the magnitude and direction of ground site pointing vector for any given time from the satellite. Lastly the time dependent SPA between the sun vector and the ground-site vector with respect to the satellite is calculated using the definition of a dot product (generalized as θ, u and v respectively in Equation 6).

$$\theta = \arccos\left(\frac{u \cdot v}{\|u\| \, \|v\|}\right) \tag{6}$$

The amount of solar flux directed back towards the ground site will vary significantly by the solar phase angle (SPA). The SPA is the angle between the Sun, satellite and ground site as shown in Fig. 1. Large phase angles correlate to back illuminated satellite poses where the back face of the solar panels are visible to the ground site.

The illumination angle (IA) is angle between the vector pointing from the ground site to the Sun (aka "Sun position vector" with respect to the ground site) and the local surface normal vector. Once these vectors are determined, the IA is calculated using Equation 6 for a given time. Notably this angle is 90° when the Sun is on the horizon and 0° when the sun is at local zenith. This angle will be used to define local sky-radiance background conditions for a given date and time. When the sun is below the local horizon, the sky is "dark" and thus no albedo from the Earth will be incident on the satellite in orbit. When the IA is between 270° and 90°, the sun will be beneath the local horizon. The sun is considered to be at 0° IA when directly overhead at the local zenith.

2.1.4 Satellite Material Reflectances

Black-body radiation from the Sun impinges on the surface of a satellite and is reflected off various satellite surfaces in both specular and diffuse (Lambertian) proportions called the Bidirectional Reflectance Distribution Function (BRDF). Surface reflection depends on both the viewing direction and illumination direction as well as the material reflectivity [12]. The BRDF is a measurement of the specularness (or directionality)

of a signal reflected off given surface. As a first-order approximation, the model generated in this research will assume spectrally dependent Lambertian reflections off all satellite surfaces. Specifically, three material spectral reflectances were approximated using empirical data: 1) kapton bus [14] 2) solar panel front (with anti-reflective coating) [7] and 3) solar panel back [5]. Each material has a spectral reflectance given in Fig. 2.

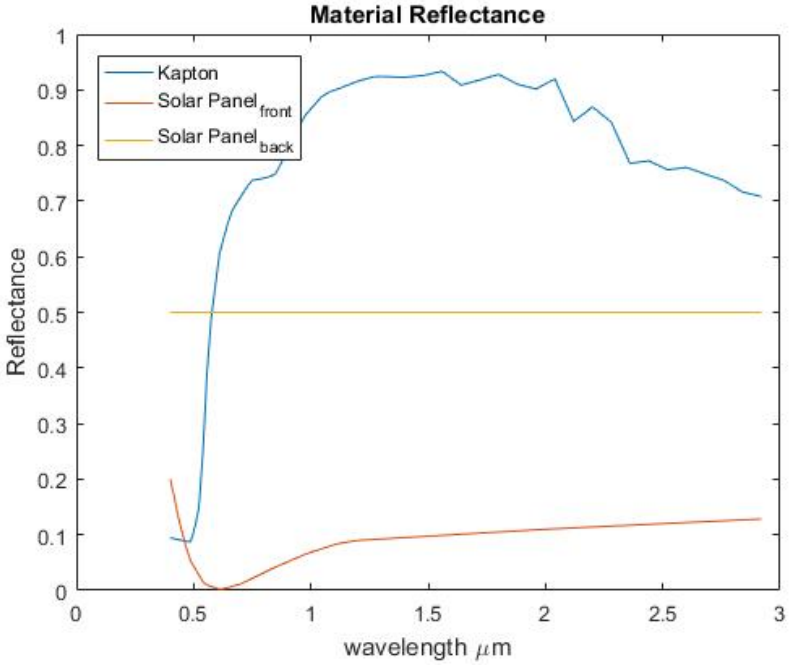

Figure 2: Material Spectral Reflectance for BoxSat

2.1.5 Projected Surface Area

To calculate the received spectral irradiance at the ground site, it is useful to consider a typical GEO satellite geometry and configuration as reference in section 2.1.4 called "BoxSat". Active GEO satellites are typified by a long, planar solar panel structure (sometimes called "solar wings") with a box-like satellite bus near their center [5]. Pertinent BoxSat assumptions include a rectangular-shaped satellite bus coated with unwrinkled mylar, Sun-tracking solar arrays, bus dimensions of 3.3 x 1.9 x 1.5 m and a solar array span of 12.6 m based on the on-orbit dimensions of the Galaxy 14 satellite [10]. Although GEOsats are often observed with varying degrees of solar panel offset from Sun-tracking [13], this model will assume Sun-tracking as an initial conservative estimate.

2.1.6 Radiation Directed Towards Ground-Site

The direct and indirect portions of the incident radiation are propagated from the satellite back towards the ground site. The amount of reflected energy is dependent on SPA, satellite pose, projected surface area, spectral surface material reflectance and atmospheric attenuation of the signal from the satellite to the detector.

2.1.7 Observed Daytime GEO Signal

For each time step (and corresponding satellite pose, projected area, SPA, and IA) the anticipated spectral irradiance (E) in Dayton, OH can be estimated by considering the satellite as a point source of known radiant flux (Φ) at a distance r, from the ground site to GEO as seen in Equations 7, and 8. This signal is

then scattered and attenuated along the slant path through the atmosphere. The net result of the satellite signal is shown in part (B) of Figs. 4, 5, 6, 7, 8 & 9.

$$I_\lambda = \frac{\Phi_{total}}{4\pi} \qquad [\mathrm{W\,\mu m^{-1}}] \quad (7)$$

$$E_\lambda = \frac{I_\lambda}{r^2} \qquad [\mathrm{W\,m^{-2}\,\mu m^{-1}}] \quad (8)$$

2.2 Sky Background Radiance Modeling

Laser Environmental Effects Definition and Reference (LEEDR) is an atmospheric characterization and radiative transfer code that calculates line-by-line (point-wise solutions for specific wavelengths) and spectral band solutions by creating "correlated, physically realizable profiles of meteorological and environmental effects (e.g. gaseous and particle extinction, optical turbulence, and cloud free line of sight) data" [6]. LEEDR has the ability to generate realistic atmospheric profiles from probabilistic climatology or observations and forecasts from numerical weather prediction models [17] and atmospheric attenuation models. LEEDR models closely mirror the atmospheric conditions on a given date and thus provide a realistic approximation of the spectral sky radiance and atmospheric transmission [17]. GEO satellites are at an altitude of approximately 35,786 km above ground level (AGL). However, atmospheric effects above 100 km AGL are considered negligible to extend the profile to GEO.

2.2.1 SWIR Atmospheric Modeling

Daytime sky brightness measurements of the GEO-belt in the NIR and SWIR do exist [8]. However, premiere imaging locations such as Haleakala, HI [8] have exceptionally clear skies with comparatively less scattering. To better understand the limitations of more ubiquitous imaging locations, Dayton, OH was selected as a representative model location. Imaging locations with greater aerosol counts will have increased scattering effects in both the visible and near-infrared (Vis-NIR) bands resulting in higher sky background radiance noise and thereby decreasing signal detectability [1]. Dayton's sky will provide a conservative estimate of bright daytime sky for comparison. The "GEO-belt" is understood to be shorthand for the orbital ring of satellites at approximately 0° inclination and zero eccentricity that have the same orbital period as the Earth's rotational period. In this research the spectral sky radiance or "brightness" is modeled throughout the day using the Global Aerosol Data Set (GADS). GADS provides aerosol constituent number densities on a 5°x 5°worldwide grid. LEEDR mapping software allows the operator to choose from specific site or regional upper air data to characterize correlated molecular absorption, aerosol absorption and scattering by percentile. Simulation of the GEO-belt in the Dayton, OH sky on 01 Jun 2018 is shown in Fig. 3 with approximate locations of the GEO-belt Meridian point (Az: 180°, El: 44°), Mid-point (Az: 220°, El: 36°), and Horizon Point (Az: 260°, El:5°). Part (C) of Figs. 4 & 5 show the the meridian point sky radiance; part (C) of Figs. 6 & 7 show the the midpoint sky radiance; and part (C) of Figs. 8 & 9 show the horizon point sky radiance.

2.3 Diffuse Signal to Noise Ratio (SNR) Modeling

The purpose of the following models are to determine are the best spectral bands to image daytime satellites of approximate size from a representative ground site such as Dayton, OH. Notably, the diffuse approximation for reflection off the satellite surface is a conservative estimate as real-world surfaces are a combination of both specular and diffuse components. Part (D) of Figs. 4, 5, 6, 7, 8 & 9 show the comparison of a generalized satellite signal model to representative sky brightness based on atmospheric constituency and historical averages. By assuming a background limited detection scenario, the "noise" or fluctuation of the sky-background radiance was assumed to be proportional to the square root of the background radiance. By converting the satellite signal and sky background radiances to photon fluxes via Eqn. 9, it is possible to assume a SNR for background limited detection per wavelength using Eqn. 10 below.

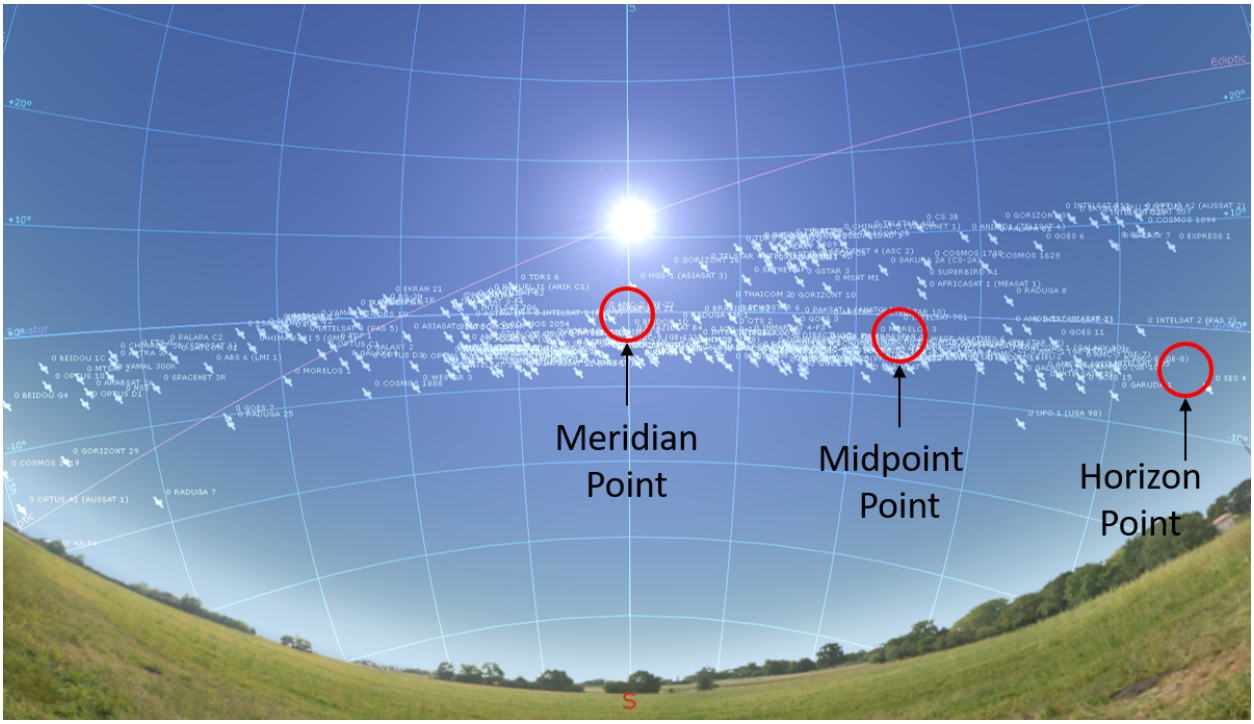

Figure 3: Simulation of the GEO-belt in the Dayton, OH sky on 01 Jun 2018. White labels represent GEO-satellites in view of the ground-site at midday. Approximate locations of Meridian point (Az:180°, El:44°), Mid-point (Az: 220°, El:36°), Horizon Point (Az:260°, El:5°) are shown in red.

$$E_{photon} = \frac{hc}{\lambda} \tag{9}$$

$$SNR = \frac{signal}{noise} = \frac{signal}{\sqrt{background}} \tag{10}$$

3 CONCLUSIONS AND FUTURE WORK

This work successfully generated a comprehensive model which quantifies SWIR contribution to daylight custody mission in terms of SNR. This model uses a conservative signal from a diffuse BoxSat accounting for solar phase angle, satellite pose and geometry as well as spectral dependence of the surface material reflection. The sky background radiance was modeled via LEEDR using the GADS database for average atmospheric conditions for a particular date from Dayton, OH including relative humidity and elevation.

The purpose of these models was to compare the SNR across bands from twilight to twilight to determine what advantages a SWIR sensor may have over a visible sensor for daytime custody. Even with a conservative satellite signal model and averaged atmospheric background, some initial conclusions from comparing parts (D) of Figs. 4, 5, 6, 7, 8 & 9 are possible:

- SNRs drop significantly as the Sun approaches the mid-day for all positions, thus true daytime custody may not be feasible much beyond twilight without sophisticated dim target methods
- Horizon SNRs (Figs. 8 & 9) are significantly lower than other orbital position SNRs (Figs. 4, 5, 6 & 7) implying that daytime custody for GEOs near the local horizon will be significantly more challenging. Increased atmosphere along the slant path both attenuates the satellite signal and increases the scattering effects thereby brightening the sky and further reducing the SNR.

- SNRs in H-band (1.5 to 1.8μm) & K-band (2.0 to 2.4μm) are more promising than visible band (0.4 to 0.7μm) near twilight.
- GEO-belt sky position/slant path has significant effect on SNR even for the same time of interest (i.e. Part (D) of Figs. 4, 6 & 8, thus "it matters where you look").
- Time of day, time of year, and satellite pose all significantly effect SNR even for the same GEO-belt position (i.e. Part (D) of Figs. 4 & 5, thus "it matters when you look").
- Higher SNRs persist in the winter twilight vs summer twilight (i.e. Part (D) of Figs. 4, 6 & 8 versus Part (D) of Figs. 5, 7 & 9). This phenomena combined with longer nights and shorter days in the winter is yet another reason why winter custody may be easier to achieve than custody of similar satellites during the summer.
- There is notably asymmetry between Sunrise and Sunset conditions in terms of detectability for part (D) of Figs. 5, 6, 7, 8 & 9, but particularly in the winter meridian point case as in part (D) of Fig. 4.

In terms of signal analysis from parts (B) of Figs. 4, 5, 6, 7, 8 & 9, it is clear that there clear dependence on solar phase angle (and thus satellite pose for sun-tracking solar arrays) and the magnitude of radiance directed towards the ground site. As an example, in Fig. 4, the SNR drops dramatically at all wavelengths near Astronomical twilight (1121 UTC) but remains relatively constant through Sunrise (1257 UTC) until approximately 1400 UTC with the highest SNR's occurring in the SWIR. The sudden drop in SNR at 1400 UTC can be attributed to the large phase angle which results in a satellite backlit case wherein the primary detectable signal from the satellite is due to Earth's albedo vice direct reflection from the Sun off the satellite solar panels.

In terms of sky background radiance, the models show that the sky radiance increases as the Sun passes closer to the GEO-belt position. Notably, part (C) of Figs. 4 & 5 occurs nearly at midday, while the peak sky background intensity is slightly shifted to later in the day for the midpoint as in part (C) of Figs. 4 & 5.

Future research will work to validate the SNRs of Figs. 4, 5, 6, 7, 8 & 9 part (D) with NIR/SWIR measurements. One key aspect to this validation will be to increase the signal and background model fidelities respectively. For the signal, modeling actual bus features such as antennas and incorporating a bi-reflectance distribution function (BRDF) for specular reflections from an increased number of satellite materials is a logical next step. The sky background radiance accuracy could also be increased by incorporating numerical weather data and atmospherics from LEEDR.

In summary, the models of Figs. 4, 5, 6, 7, 8 & 9 indicate that SWIR-band imaging offers some distinct advantages to daylight custody. These models also show that time of year, time of day, and satellite position in the sky all impact the SNR and thus quality of images one can expect. This research does indicate that higher SNR values persist in the SWIR beyond the Visible-NIR near twilight for short periods. However, in the most conservative case, imaging all day in the SWIR may not be possible as the SNR level fades into the noise across all wavelengths from this location and diffuse satellite signal. Within the limits of a sensor and dim target detection algorithms, this additional detection period during twilight may be exploited to extend GEO satellite daytime custody. Persistent SWIR imaging throughout twilight hours is relatively inexpensive to implement (as compared to LWIR or radar imaging for example) and thus has the potential to significantly increase the ground-based GEO custody window as compared to using Vis-NIR detectors alone.

ACKNOWLEDGMENTS

The authors would like to thank Brannon Elmore (AFIT), Dr. Steve Fiorino (AFIT) and Dr. Mike Hawks (AFIT) for technical consultation on the model development.

REFERENCES

[1] Michael C B Ashley et al. "South Pole Observations of the Near-Infrared Sky Brightness". In: *Publications of the Astronomical Society of the Pacific* 108 (1996), pp. 721–723.

[2] Charlie T Bellows. "Leveraging External Sensor Data for Enhanced Space Situational Awareness". PhD thesis. Air Force Institute of Technology, 2015.

[3] R.W. Boyd. *Radiometry and the Detection of Optical Radiation*. New York: John Wiley and Sons, 1983.

[4] Chairman of Joint Chiefs of Staff. *Joint Publication 3-14, Space Operations*. Tech. rep. Department of Defense, 2013.

[5] Rita L Cognion. "Large Phase Angle Observations of GEO Satellites". In: *SPIE* 8739.10 (2013). DOI: 10.1117/12.2014623.

[6] Donna Courtney. *What's the Use? V and V of an Atmospheric Characterization and Radiative Transfer Code*. Tech. rep. 2015.

[7] Michael T. Eismann. *Hyperspectral Remote Sensing*. 1st ed. Bellingham, WA: SPIE Press, 2012, p. 748. ISBN: 9780819487889. DOI: 10.1117/3.899758.

[8] Kevin T C Jim, Brooke N Gibson, and Edward A Pier. "Daytime Sky Brightness Modeling of Haleakala along the GEO Belt". In: *Advanced Maui Optical and Space Surveillance Technologies Conference*. Wailea, Maui, Hawaii, 2012.

[9] Kevin T C Jim et al. "The HANDS-IONS Daytime Camera for GEO Satellite Characterization". In: *Advanced Maui Optical and Space Surveillance Technologies (AMOS)*. 2012.

[10] Kathryn Lancioni. *The Galaxy 14 Satellite Spec Sheet*. Tech. rep. Arianne Space, 2005, p. 7. URL: www.arianespace.com.

[11] Marc A Murison and David G Monet. *Precise Simultaneous Astrometry and Photometry of Moving Objects with an OTCCD*.

[12] Shree Nayar, Ravi Ramamoorthi, and Pat Hanrahan. *Basic Principles of Surface Reflectance*. 2009.

[13] Tamara E Payne et al. "SSA Analysis of GEOs Photometric Signature Classifications and Solar Panel Offsets". In: *Advanced Maui Optical and Space Surveillance Technologies (AMOS) Conference*. Maui, 2006.

[14] Jack Triolo. *TFAWS 2015 - Thermal Coatings Seminar Series Training*. 2015. URL: https://tfaws.nasa.gov/files/TFAWS2015-SC-Coatings-for-Thermal-Engineers-1.pdf.

[15] USSTRATCOM. *USSTRATCOM Space Control and Space Surveillance*. Tech. rep. 2014.

[16] D.A. Vallado and W.D. McClain. *Fundamentals of Astrodynamics and Applications*. Ed. by Space Technology Library. Netherlands: Springer, 2001.

[17] Nathan P. Wurst, Joseph Meola, and Steven T. Fiorino. "Improved atmospheric characterization for hyperspectral exploitation". In: *SPIE Defense + Security*. Anaheim, 2017. ISBN: 0277786X. DOI: 10.1117/12.2265853.

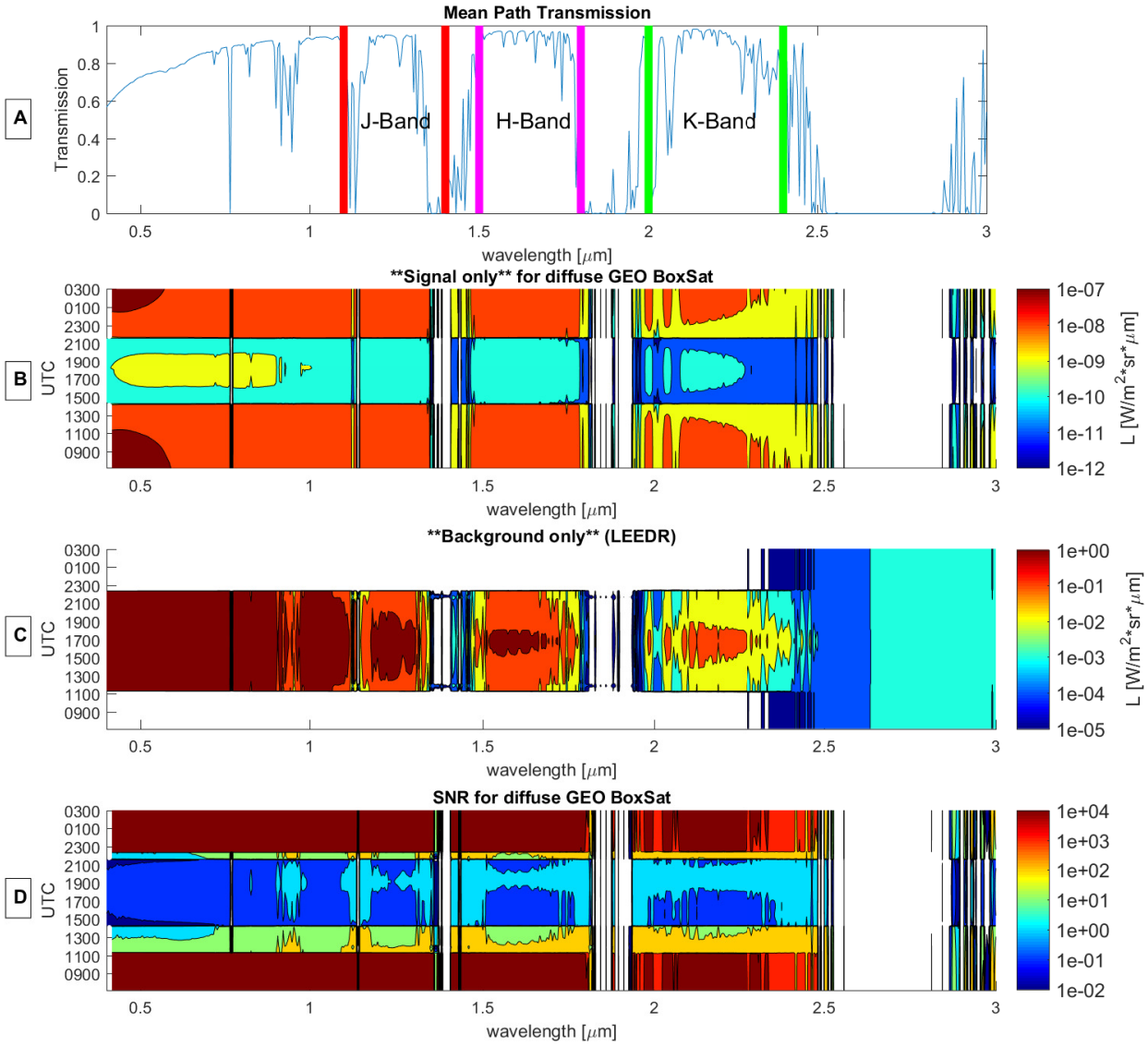

Figure 4: 01 JAN 18 - GEO-belt Meridian Point (Az: 180°, El: 44°): Transmission (A), satellite signal (B), sky background radiance (C), and signal-to-noise ratio (D) for diffuse GEO BoxSat as seen from Dayton, OH on 1/1 - 1/2/2018. Sunrise time occurred at 1257 UTC (1/1) and Sunset at 2223 UTC (1/1) for this date and location. Note: whitespace for values in parts (B),(C) and (D) indicate quantities below the minimum value of 10^{-12} $W/m^2*sr*\mu m$ for satellite signal, 10^{-5} $W/m^2*sr*\mu m$ for sky radiance and 10^{-2} for SNR respectively.

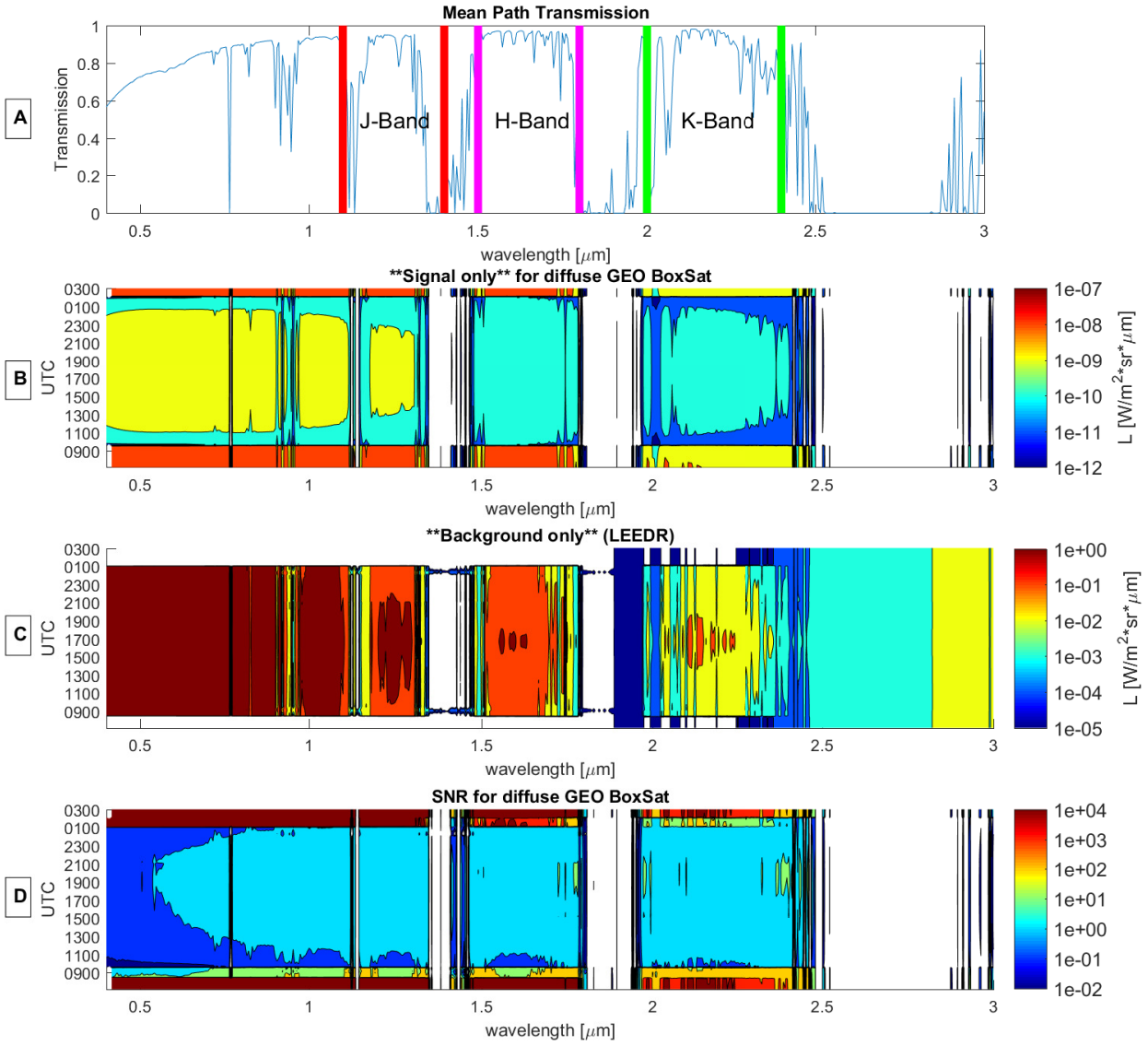

Figure 5: 01 JUN 18 - GEO-belt Meridian Point (Az: 180°, El: 44°): Transmission (A), satellite signal (B), sky background radiance (C), and signal-to-noise ratio (D) for diffuse GEO BoxSat as seen from Dayton, OH on 6/1 - 6/2/2018 . Sunrise time occurred at 1012 UTC (6/1) and Sunset at 0108 UTC (6/2). Note: whitespace for values in parts (B),(C) and (D) indicate quantities below the minimum value of 10^{-12} $W/m^2 *sr*\mu m$ for satellite signal, 10^{-5} $W/m^2 *sr*\mu m$ for sky radiance and 10^{-2} for SNR respectively.

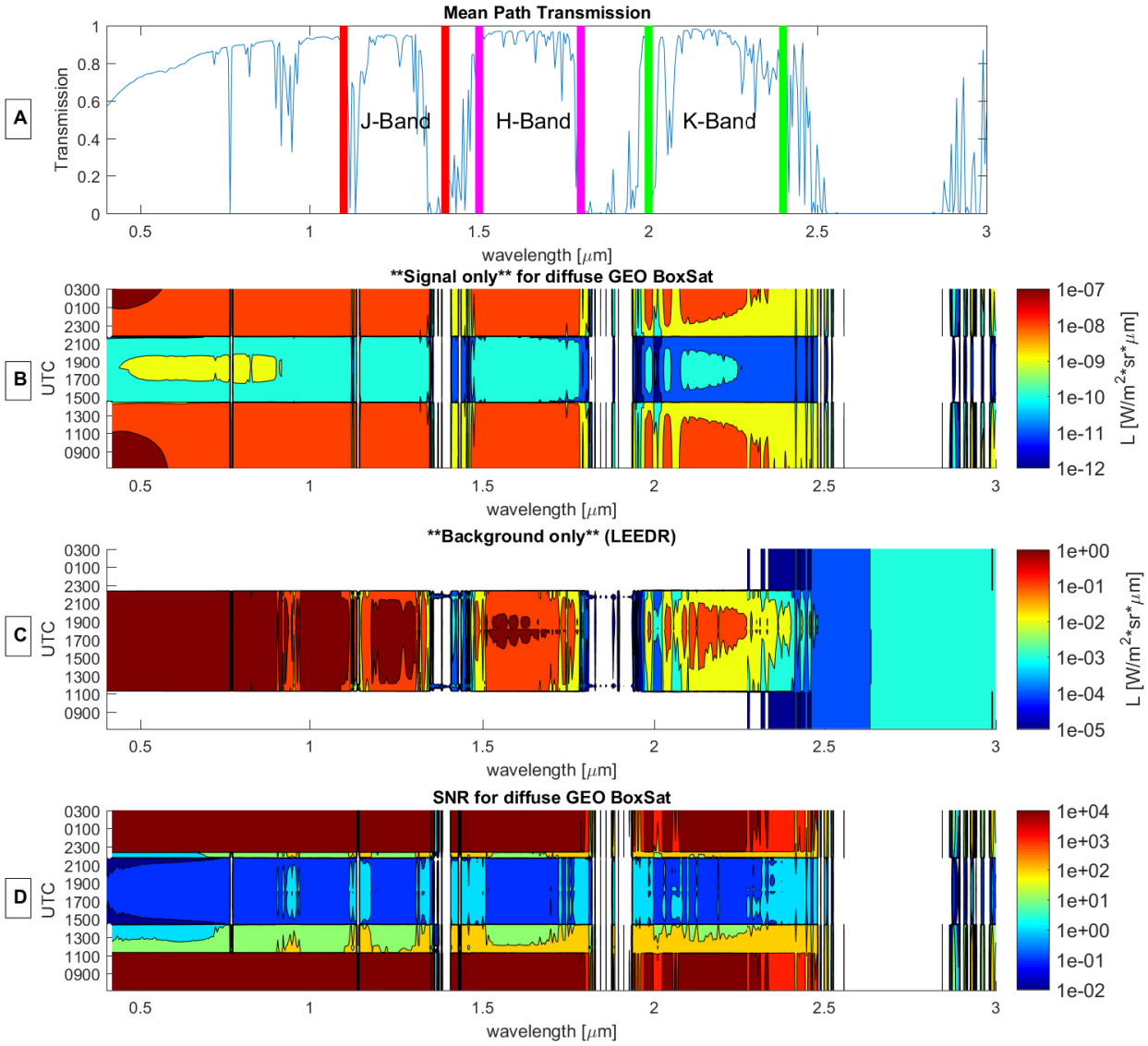

Figure 6: 01 JAN 18 - GEO-belt Midpoint (Az: 220°, El: 36°): Transmission (A), satellite signal (B), sky background radiance (C), and signal-to-noise ratio (D) for diffuse GEO BoxSat as seen from Dayton, OH on 1/1 - 1/2/2018. Sunrise time occurred at 1257 UTC (1/1) and Sunset at 2223 UTC (1/1) for this date and location. Note: whitespace for values in parts (B),(C) and (D) indicate quantities below the minimum value of 10^{-12} $W/m^2*sr*\mu m$ for satellite signal, 10^{-5} $W/m^2*sr*\mu m$ for sky radiance and 10^{-2} for SNR respectively.

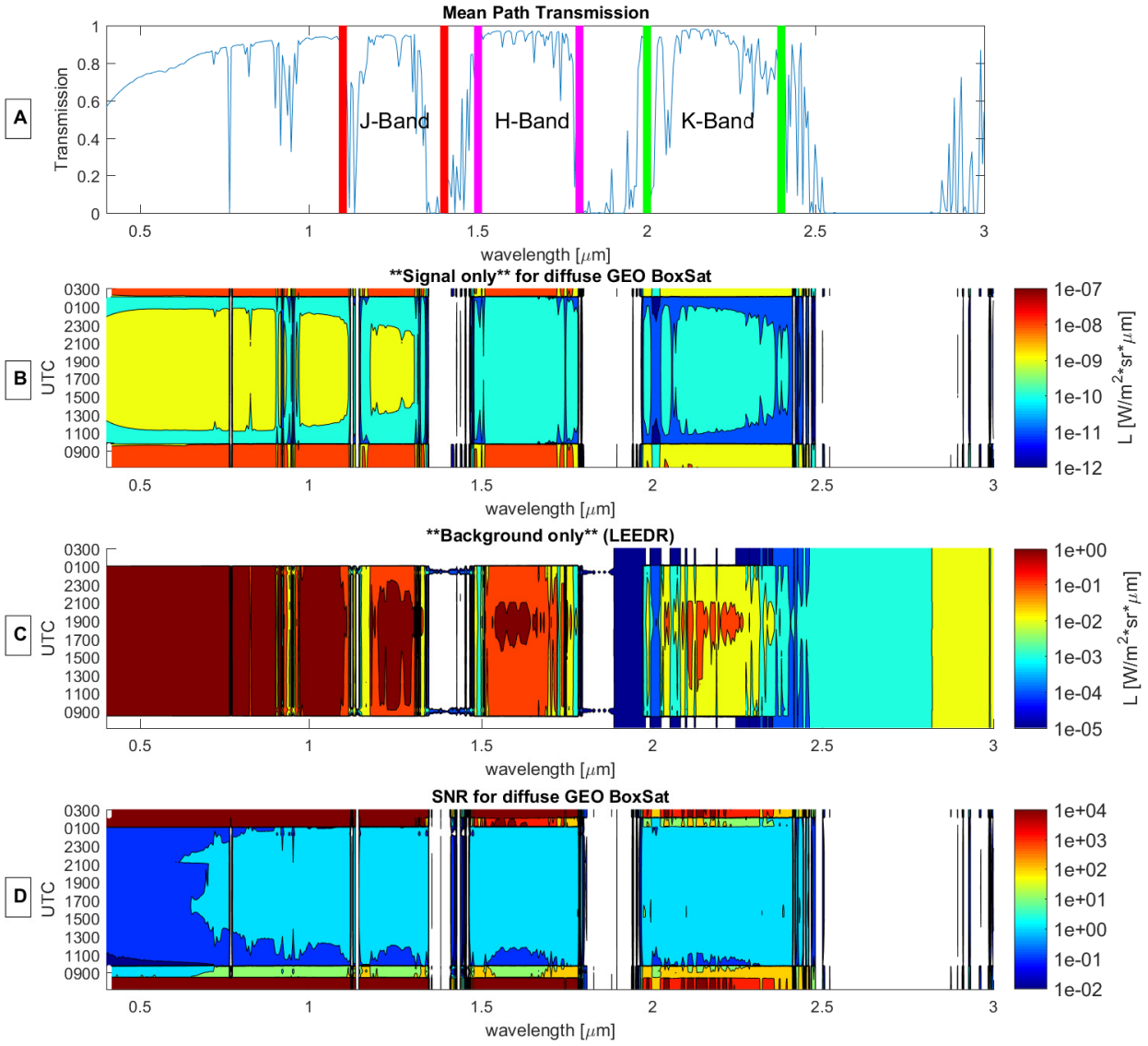

Figure 7: 01 JUN 18 - GEO-belt Midpoint (Az:220°, El:36°): Transmission (A), satellite signal (B), sky background radiance (C), and signal-to-noise ratio (D) for diffuse GEO BoxSat as seen from Dayton, OH on 6/1 - 6/2/2018 . Sunrise time occurred at 1012 UTC (6/1) and Sunset at 0108 UTC (6/2). Note: whitespace for values in parts (B),(C) and (D) indicate quantities below the minimum value of 10^{-12} $W/m^2*sr*\mu m$ for satellite signal, 10^{-5} $W/m^2*sr*\mu m$ for sky radiance and 10^{-2} for SNR respectively.

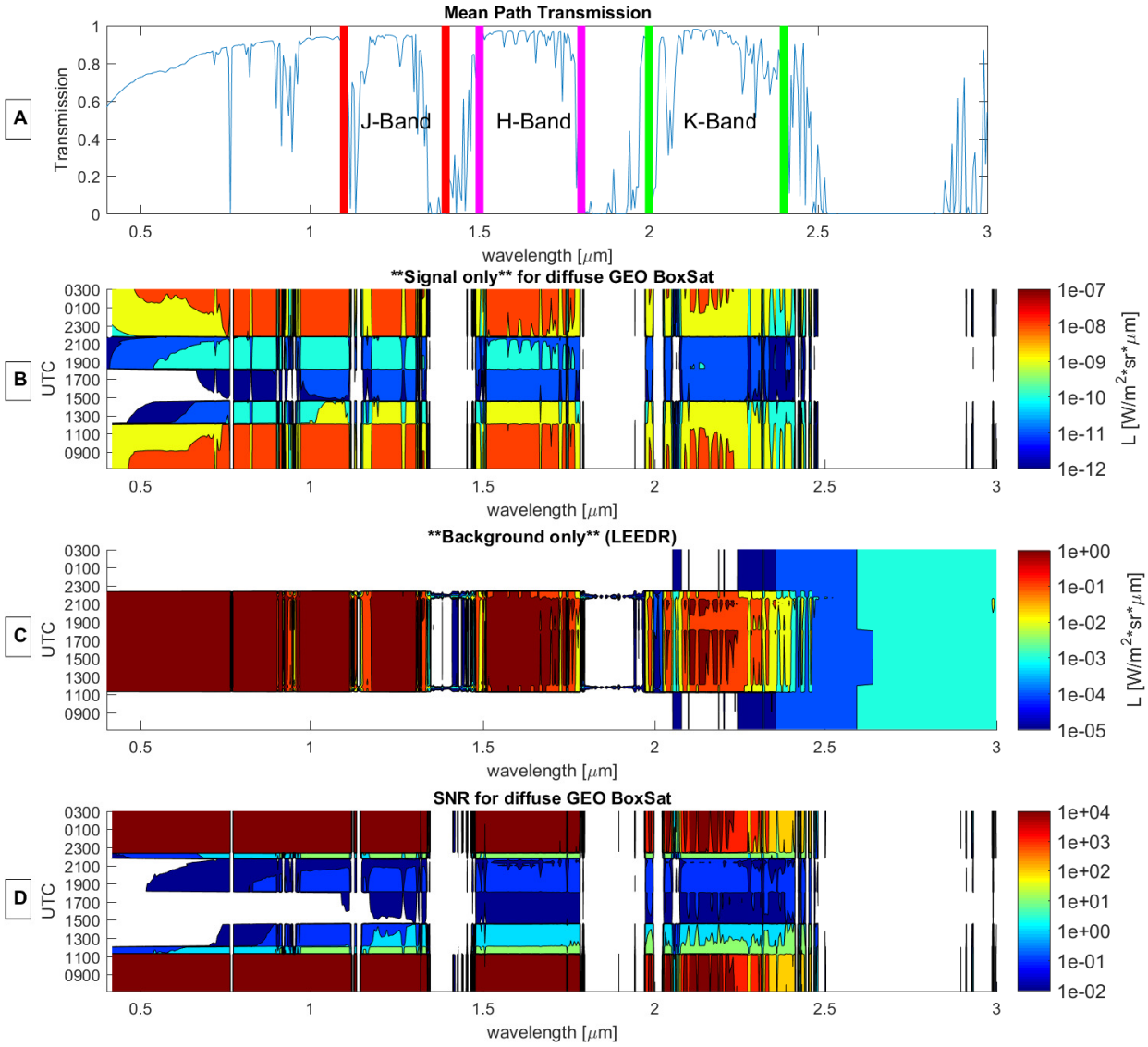

Figure 8: 01 JAN 18 - GEO-belt Horizon Point (Az:260°, El:5°): Transmission (A), satellite signal (B), sky background radiance (C), and signal-to-noise ratio (D) for diffuse GEO BoxSat as seen from Dayton, OH on 1/1 - 1/2/2018. Sunrise time occurred at 1257 UTC (1/1) and Sunset at 2223 UTC (1/1) for this date and location. Note: whitespace for values in parts (B),(C) and (D) indicate quantities below the minimum value of 10^{-12} $W/m^2*sr*\mu m$ for satellite signal, 10^{-5} $W/m^2*sr*\mu m$ for sky radiance and 10^{-2} for SNR respectively.

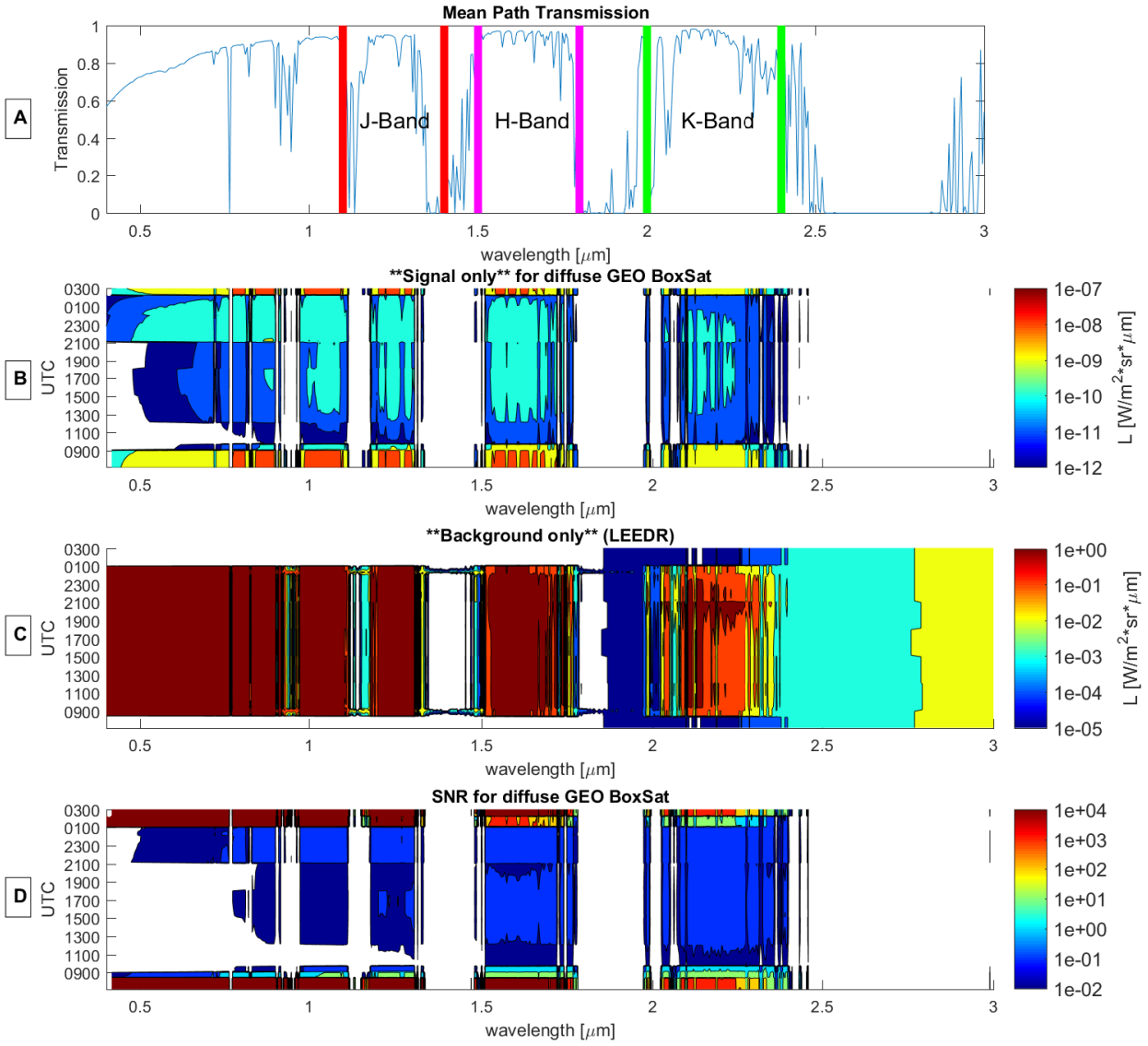

Figure 9: 01 JUN 18 - GEO-belt Horizon Point (Az:260°, El:5°): Transmission (A), satellite signal (B), sky background radiance (C), and signal-to-noise ratio (D) for diffuse GEO BoxSat as seen from Dayton, OH on 6/1 - 6/2/2018 . Sunrise time occurred at 1012 UTC (6/1) and Sunset at 0108 UTC (6/2). Note: whitespace for values in parts (B),(C) and (D) indicate quantities below the minimum value of 10^{-12} $W/m^2 *sr*\mu m$ for satellite signal, 10^{-5} $W/m^2 *sr*\mu m$ for sky radiance and 10^{-2} for SNR respectively.